Coverage and Distance Optimization for Interference-Aware NR-FSS Coexistence

Amina Girdher, Nishant Gupta, Jun-Bae Seo, Swades De, and Ranjan K. Mallik

***Abstract*—The increasing demand for new radio (NR) deployment in the C-band has raised significant concerns about co-channel interference with incumbent fixed satellite services (FSS). This paper investigates an interference-aware coexistence strategy leveraging NR flexibility such that the signal-to-interference-and-noise ratio (SINR) at the earth station (ES) remains above a predefined threshold. Considering full use of the available NR BS subcarriers, the minimum distance from the NR base stations (BSs) to the FSS ES is optimized to maximize the NR and FSS performance and optimize the coverage radius of the NR BS. The resulting optimization problem is solved through an iterative search-based approach, considering the performance of both NR and FSS networks. Simulation results show the efficacy of leveraging NR flexibility. This study provides actionable design guidelines for spectrum regulators and network planners to enable harmonious coexistence of terrestrial and satellite systems.**

***Index Terms*—C-band, DVB-S2, in-band coexistence, fixed satellite services, new radio**

I. Introduction

THE exponential growth in cellular data traffic has driven aggressive deployment of new radio (NR) systems in the mid-band spectrum (C-band). However, the C-band is extensively utilized by incumbent fixed satellite services (FSS) for downlink communications to earth stations (ESs), raising significant co-channel interference concerns. Given spectrum scarcity, enabling in-band coexistence between NR and FSS while maintaining performance and quality of service (QoS) for both systems poses a considerable challenge.

To enable in-band coexistence between FSS and terrestrial networks, the International Telecommunication Union recommended large protection distances, typically 20 km for an ES with a 36° elevation angle, to prevent harmful interference from IMT-Advanced base stations (BSs) [1]. Such conservative measures restrict NR growth. Therefore, finding reduced optimal NR BS to ES distances that balance incumbent protection with NR expansion is critical. To reduce protection distances, RF filtering at the low noise block (LNB) and successive interference cancellation were proposed in [2] and [3], respectively. However, these require significant FSS ES hardware modifications, posing major challenges for deployed systems.

Besides the above approaches, guard band-based interference control was studied in [4], [5] for improved coexistence between NR and FSS, where the impact of guard bands and signal arrival angles on the protection distances were also analyzed. Adaptive beamforming and active antenna at terrestrial BSs were explored to limit FSS interference [6]–[8]. While reducing protection distance requirements, they constrain network deployment by necessitating alternative coverage for areas outside beam footprints. Multi-access schemes, including non-orthogonal multi-access and rate-splitting multi-access, have been employed in [9]–[11] to improve spectral efficiency, though complexity escalates with user density. These solutions depend on dynamic coordination and hardware upgrades in both networks, making them impractical for legacy systems. Moreover, these works [6]–[11] addressed coexistence through component-wise interference reduction. While contributing to interference mitigation, network-level optimization strategies jointly accounting for both systems' characteristics and constraints largely remain unexplored.

Unlike previous works, this paper focuses on one-sided adaptation for NR-FSS coexistence. By exclusively adapting NR parameters, legacy FSS ESs are procted without requiring changes to hardware or reception capabilities, offering a practical, backward-compatible solution for real-world deployment. Two key questions are addressed: (i) What minimum NR BS to ES distance ensures acceptable performance for both systems? (ii) Given fixed separation, what maximum NR coverage radius satisfies user rate constraints while protecting the ES?

II. in-band Coexistent System Model

We consider a spectrum sharing scenario where a terrestrial NR network operates in the same C-band frequencies as FSS downlink, as shown in Fig. 1, with both systems transmitting simultaneously within overlapping frequency bands, creating mutual interference. The FSS system comprises a satellite transmitter employing the DVB-S2 standard and a fixed Earth Station (ES) receiver located at $\mathcal{X}^{\mathrm{U}} = [x_F, y_F, z_F]$. The satellite transmits a multiple-channel-per-carrier (MCPC) time division multiplexed (TDM) signal. The terrestrial NR network consists of K BSs, each serving M active users. BSs are arranged linearly, with the k-th BS located at $\mathcal{X}_k^{\mathrm{BS}} = [x_k^{\mathrm{BS}}, y_k^{\mathrm{BS}}, z_k^{\mathrm{BS}}]$ and each user at $\mathcal{X}_{k,m}^{\mathrm{NR}}$. Due to spectral overlap, NR downlink signals interfere with ES reception, while satellite downlink has negligible interference to NR users [12]. While the study focuses on a single-ES case for clarity, it can be extended to multi-ES protection scenarios.

This work was supported in part by THDC under grant THDC/RKSH/R&D/F-2076/1036, in part by the ANRF, DST, Government of India, under grant CRG/2023/005421, in part by ANRF, DST, Government of India, under the J. C. Bose Fellowship, and in part by DRDO, Government of India, under the grant DFTM/03/3203/M/01/IATC/2026/D(R&D).

A. Girdher is with the Department of ECE, NIT Jalandhar, Jalandhar, India (e-mail: girdher.amina@gmail.com). N. Gupta is with the Department of Communication and Computer Engineering, The LNMIIT Jaipur, Jaipur, India (e-mail: nishantgupta.nic@gmail.com). J.-B. Seo is with the Department of Artificial Intelligence and Information Engineering, Gyeongsang National University, Jinju 53064, Republic of Korea (e-mail: jbseo@gnu.ac.kr). S. De and R. K. Mallik are with the Department of Electrical Engineering, IIT Delhi, New Delhi, India (e-mail: swadesd@ee.iitd.ac.in, rkmallik@ee.iitd.ernet.in).

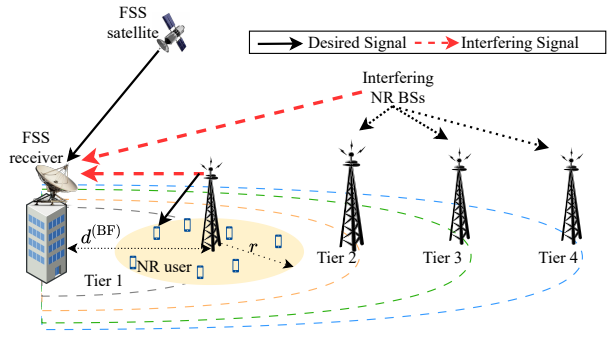

Fig. 1: In-band coexistent FSS and NR system model in C-band.

A. Transmission signals of DVB-S2 and NR

The MCPC TDM-based DVB-S2 broadcast signal transmitted by the satellite transmitter is given by $x^{(\mathrm{F})}(t) = \sqrt{G_T^{(\mathrm{F})} P_T^{(\mathrm{F})}} \sum_{s=0}^{S-1} a_s p\left(t - sT^{(\mathrm{F})}\right)$, where $G_T^{(\mathrm{F})}$ is the satellite transmitting antenna gain, $P_T^{(\mathrm{F})}$ the transmit power, S the number of symbols transmitted, $p(t)$ the energy-normalized squared root raised cosine (SRRC) filter, a_s the random s-th modulated symbol. The symbol period is $T^{(\mathrm{F})} = \frac{1}{\mathcal{R}^{(\mathrm{F})}}$, with symbol rate $\mathcal{R}^{(\mathrm{F})} = \mathcal{B}^{(\mathrm{F})}/(1+\alpha)$, where $\mathcal{B}^{(\mathrm{F})}$ is the bandwidth of FSS downlink and α the roll-off factor. The time-domain SRRC filter is given by $p(t) = \left[4\alpha \cos\left((1+\alpha)\frac{\pi t}{T^{(\mathrm{F})}}\right) + \sin\left((1-\alpha)\frac{\pi t}{T^{(\mathrm{F})}}\right)\frac{T^{(\mathrm{F})}}{t}\right] / \left[\pi\sqrt{T^{(\mathrm{F})}} \times \left(1 - \left(\frac{4\alpha t}{T^{(\mathrm{F})}}\right)^2\right)\right]$. The signal transmitted by the k^{th}-NR BS to its the m^{th}-associated user can be expressed as

$$x_{k,m}^{(\mathrm{N})}(t) = \frac{1}{\sqrt{T_u^{(\mathrm{N})}}} \sum\nolimits_{\ell\in\mathbb{Z}} \sum\nolimits_{n=0}^{N-1} \delta_{k,m,n} X_{k,m}^{(\mathrm{N})}[\ell,n] e^{\frac{j2\pi nt}{T_u^{(\mathrm{N})}}} \times \mathrm{rect}\left(\frac{t - \ell T_u^{(\mathrm{N})} + T_g^{(\mathrm{N})}}{T_{\mathrm{tot}}^{(\mathrm{N})}}\right), \quad (1)$$

where N is the number of OFDM subcarriers. The total OFDM symbol duration is $T_{\mathrm{tot}}^{(\mathrm{N})} = T_u^{(\mathrm{N})} + T_g^{(\mathrm{N})}$, with $T_u^{(\mathrm{N})}$ and $T_g^{(\mathrm{N})}$ being the useful symbol and cyclic prefix durations, respectively. For the k^{th}-NR BS, $\delta_{k,m,n}$ is an indicator function that equals 1 if the n^{th}-subcarrier is assigned to the m^{th}-user, and 0 otherwise. $X_{k,m}^{(\mathrm{N})}[\ell,n]$ is the transmitted data symbol for OFDM block ℓ on subcarrier n, with average power $P_{k,m,n}^{(\mathrm{N})} = \mathbb{E}[|X_{k,m}^{(\mathrm{N})}[\ell,n]|^2]$. $\mathrm{rect}(t) = 1$, when $0 \le t \le 1$, and 0, otherwise.

B. Signal Received at FSS and NR Receivers

The signal received at the FSS receiver is given by

$$y^{(\mathrm{F})}(t) = \sqrt{G_R^{(\mathrm{F})}}\mathcal{H}^{(\mathrm{F})}(t) * x^{(\mathrm{F})}(t) + \sum\nolimits_{k=1}^{K} \sqrt{\tilde{G}_{R,k}^{(\mathrm{F})}}\mathcal{H}_k^{(\mathrm{BF})}(t) * \sum\nolimits_{m=1}^{M} x_{k,m}^{(\mathrm{N})}(t) + n^{(\mathrm{F})}(t), \quad (2)$$

where $*$ denotes the convolution, $G_R^{(\mathrm{F})}$ is the gain of the ES antenna toward the satellite transponder, and $\tilde{G}_{R,k}^{(\mathrm{F})}$ is ES antenna gain toward the k-th NR BS. $\mathcal{H}^{(\mathrm{F})}(t)$ represents the satellite to SE receiver channel impulse response (CIR): $\mathcal{H}^{(F)}(t) = \sum_{i=1}^{L_1} h_i^{(F)} \delta(t - \tau_i^{(F)})$, where $\tau_i^{(F)}$ is the delay of the i-th multipath component for a total of L_1 paths, and $h_i^{(F)} = \tilde{h}_l \hat{h}_a \tilde{h}_{f,i}^{(F)}$ with $|\tilde{h}_l|^2 = c^2(4\pi R_E f_c^{(\mathrm{F})})^{-2}$, (free-space loss, c being the speed of light, R_E the path length, $f_c^{(\mathrm{F})}$ the carrier frequency). While $\hat{h}_a$ models the atmospheric absorption loss, $\tilde{h}_{f,i}^{(F)}$ is the multipath fading following $\mathrm{Nakagami}(m^{(F)}, \Omega^{(F)})$. The CIR from the k^{th}-NR BS to the ES receiver in (2) is $\mathcal{H}_k^{(\mathrm{BF})}(t) = \sum_{i=1}^{L_2} q_i^{(k)} \delta(t - \tau_i^{(k)})$, where $q_i^{(k)} = \tilde{q}_l^{(k)} \tilde{q}_{f,i}^{(k)}$, $\tilde{q}_l^{(k)} = P_{\mathrm{LoS}}^{(k)} q_{l,\mathrm{LoS}}^{(k)} + (1 - P_{\mathrm{LoS}}^{(k)}) q_{l,\mathrm{NLoS}}^{(k)}$ models large-scale fading with LoS probability $P_{\mathrm{LoS}}^{(k)}$ [13], and $\tilde{q}_{f,i}^{(k)} \sim \mathrm{Nakagami}(m^{(k)}, \Omega^{(k)})$ models small-scale fading of Nakagami-m distribution. Finally, $n^{(\mathrm{F})}(t)$ in (2) is additive white Gaussian noise (AWGN) at the input of the ES receiver.

The matched filter $p_{MF}(t) = p(T^{(\mathrm{F})} - t)$ at the ES processes the received signal $y^{(\mathrm{F})}(t)$ as $y^{(\mathrm{F})}(t) * p_{\mathrm{MF}}(t)\big|_{t=T^{(\mathrm{F})}} = \tilde{a}_s + \sum_{k=1}^{K} I_{s,k} + n_s$, where the noise contribution is $n_s = N_o^{(\mathrm{F})} \mathcal{B}^{(\mathrm{F})}$ with power spectral density of AWGN $N_o^{(\mathrm{F})}$ and bandwidth of the FSS network $\mathcal{B}^{(\mathrm{F})}$, and $\tilde{a}_s$ is the desired s-th FSS symbol given by $\tilde{a}_s = \mathcal{A}_1 \mathcal{H}^{(\mathrm{F})}(t) a_s$, where $\mathcal{A}_1 = \sqrt{G_T^{(\mathrm{F})} G_R^{(\mathrm{F})} P_T^{(\mathrm{F})}}$. The interference from the k-th NR BS to the s^{th} FSS symbol, denoted by $I_{s,k}$, is given by $I_{s,k} = \sqrt{\tilde{G}_{R,k}^{(\mathrm{F})}} \mathcal{H}_k^{(\mathrm{BF})}(t) \int_0^{T^{(\mathrm{F})}} \sum_{m=1}^{M} x_{k,m}^{(\mathrm{N})}(\tau) p(\tau) d\tau$. The SINR at the ES receiver is then $\Gamma^{(\mathrm{F})} = \frac{\mathcal{A}_1^2 |\mathcal{H}^{(\mathrm{F})}(t)|^2}{\mathbb{E}_{X_{k,m}[\ell,n], \mathcal{H}_k^{(\mathrm{BF})}}[|I_{s,k}|^2] + N_o^{(\mathrm{F})} \mathcal{B}^{(\mathrm{F})}}$, where $\mathbb{E}_{X_{k,m}[\ell,n], \mathcal{H}_k^{(\mathrm{BF})}}\left[|I_{s,k}|^2\right]$ is the variance of $I_{s,k}$ averaged over $X_{k,m}[\ell,n]$ and $\mathcal{H}_k^{(\mathrm{BF})}(t)$.

Since our objective is to protect the FSS receiver through NR-side adaptation, we have excluded the study of inter-cell NR interference. However, the existing inter-cell interference coordination (ICIC) mechanisms can manage such interference independent of our framework. Accordingly, the signal received at the m-th user by its k-th NR BS over the n-th subcarrier is given by $y_{k,m}^{(\mathrm{N})}(t) = \mathcal{H}_{k,m}^{(\mathrm{BN})}(t) * x_{k,m}^{(\mathrm{N})}(t) + n_m^{(\mathrm{N})}(t)$, where $\mathcal{H}_{k,m}^{(\mathrm{BN})}(t)$ is the CIR from the k^{th}-NR BS to its associated users which is calculated in the same way as $\mathcal{H}_k^{(\mathrm{BF})}(t)$ for the m^{th}-user. $n_m^{(\mathrm{N})}(t)$ denotes complex Gaussian noise with zero mean and variance $N_o^{(\mathrm{N})}$. The NR receiver output is obtained by projecting the received signal $y_{k,m}^{(\mathrm{N})}(t)$ onto the OFDM basis function $\Phi_{n,\ell}^{(\mathrm{N})}(t) = \frac{1}{\sqrt{T_u^{(\mathrm{N})}}} e^{-j2\pi \frac{nt}{T_u^{(\mathrm{N})}}} \mathrm{rect}\left(\frac{t - \ell T_{tot}^{(\mathrm{N})}}{T_u^{(\mathrm{N})}}\right)$, yielding the demodulated symbol $\tilde{X}_{k,m}[n,\ell] = \int_{\mathbb{R}} y_{k,m}^{(\mathrm{N})}(t) \Phi_{n,\ell}^{(\mathrm{N})} dt = X_{k,m}[n,\ell] \mathcal{H}_{k,m}^{(\mathrm{BN})}(t)$. The SNR at the m-th user from its k-th NR BS with a subcarrier spacing of Δf_n is given by $\Gamma_{k,m,n}^{(\mathrm{N})} = \frac{P_{k,m,n}^{(\mathrm{N})} |\mathcal{H}_{k,m}^{(\mathrm{BN})}(t)|^2}{N_o^{(\mathrm{N})} \Delta f_n}$. Then, the achievable average received data rate of m-th user from its k-th NR BS is given by $\mathcal{R}_{k,m}^{(\mathrm{N})} = \sum_{n=0}^{N-1} \mathbb{E}\left[\delta_{k,m,n} \Delta f_n \log_2\left(1 + \Gamma_{k,m,n}^{(\mathrm{N})}\right)\right]$.

III. Problem Formulation

To evaluate NR-FSS coexistence, we simulate a scenario where NR BSs are deployed linearly along an axis (cf. Fig. 1) with varied BS spacings, 400 m–800 m for urban macro (UMa) scenario and 1500 m–3500 m for rural macro (RMa) scenario based on 3GPP TR 38.901 [13]. Although multiple

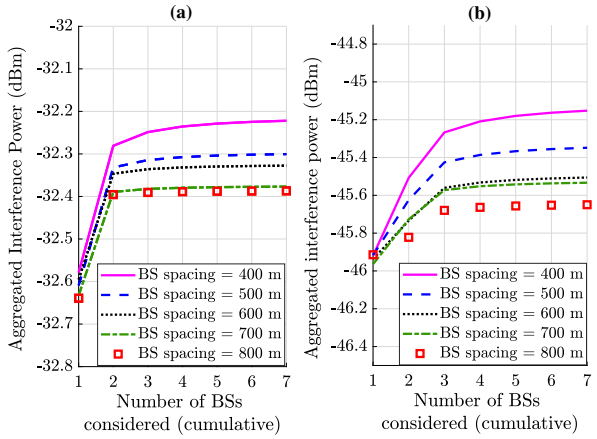

Fig. 2: Interference contribution per NR BS tier (a) rural macro (RMa) scenario and (b) urban macro (UMa) scenario.

BSs exist at the same distance (in each tier), the BS within the antenna main lobe dominates ES interference. Thus, a single BS (in each tier) aligned with the ES antenna captures the worst-case interference. From Figs. 2(a) and (b), it is evident that the interference is dominated by the nearest base station. For instance, in Fig. 2(a), when BS spacing is 1500 m, the interference from first BS alone is about –32.6 dBm. When the second BS is included, the aggregated interference increases to roughly –32.3 dBm. Thus, the second BS contributes only additional 0.3 dB interference. Even when all ten BSs are cumulatively considered, the total interference reaches around –32.25 dBm, which is only about 0.35 dB higher than the contribution from the first BS alone. A similar trend is observed in Fig. 2(b). Therefore, if an ES can tolerate interference from the closest BS, it can reasonably withstand very small additional interference generated by the BSs in higher tiers. Thus, optimizing around first BS is sufficient; accordingly in our optimization we consider only Tier-1 BS.

Our aims are twofold: 1) minimize the NR–ES distance while ensuring NR and ES performance guarantees; 2) maximize the NR BS coverage while maintaining ES protection. The BS-ES distance minimization problem is formulated as

$$\text{P1}: \underset{\mathcal{X}^{\text{U}},\delta_{m,n},P^{(N)}_{m,n},\forall m,n}{\text{minimize}} \quad d^{(\text{BF})} = \left\|\mathcal{X}^{\text{BS}} - \mathcal{X}^{\text{U}}\right\|$$
$$\text{s.t.}: (C1): \mathcal{R}^{(\text{N})}_m \geq \mathcal{R}_{Th}, \quad (C2): \Gamma^{(\text{F})} \geq \Gamma_{Th}$$
$$(C3): P^{(\text{N})}_{m,n} > 0, \quad (C4): \delta_{m,n} \in \{0,1\}, \forall m,n,$$
$$(C5): \sum_{m=1}^{M}\sum_{n=1}^{N} \delta_{m,n} \cdot P^{(N)}_{m,n} \leq P_{\max}, \; (C6): \sum_{m=1}^{M} \delta_{m,n} \leq 1, \forall n$$

where $d^{(\text{BF})}$ is the distance between the tier-1 NR BS and the ES. $(C1)$ ensures each NR user in the coverage of Tier-1 NR BS achieves a minimum data rate $\mathcal{R}_{Th}$, $(C2)$ enforces a minimum SINR Γ_{Th} at the ES, $(C3)$ and $(C5)$ represent the power allocation constraints, and $(C4)$ and $(C6)$ represents subcarrier allocation. P1 is nonconvex due to the presence of both integer variables and non-linear constraints of SINR.

To solve P1, we propose a two-stage decomposition. *Stage 1* is to fix the ES location and optimize NR transmission using one of two priority approaches as follows: *(i)* rate-prioritized approach (RPO) emphasizes the NR network data rate:

$$\text{P2}: \underset{\delta_{m,n},P^{(N)}_{m,n}}{\text{maximize}} \sum\nolimits_{m=1}^{M} \mathcal{R}^{(N)}_m, \quad \text{s.t.} \quad (C1)-(C6).$$

This maximizes the NR performance while respecting the ES interference threshold and constraints $(C3)-(C6)$. P2 is ideal when the main focus is on maximizing throughput for NR users, such as in data-intensive applications. *(ii)* SINR-prioritized approach (SPO) prioritizes SINR at the ES:

$$\text{P3}: \underset{\delta_{m,n},P^{(N)}_{m,n}}{\text{maximize}} \quad \Gamma^{(\text{F})}, \quad \text{s.t.} \quad (C1)-(C6).$$

This approach is optimal when primary systems (ES) require strong protection from secondary (NR) interference.

Stage 2 minimizes the BS–ES distance $d^{(\text{BF})}$ by optimizing the ES location $\mathcal{X}^{\text{U}}$ for a given NR transmission parameters, subject to maintaining the SINR at the ES above a specified threshold. The optimization problem is given by

$$\text{P4}: \underset{\mathcal{X}^{\text{U}}}{\text{minimize}} \quad d^{(\text{BF})} \quad \text{s.t.} \quad (C2)$$

Stages 1 and 2 are solved iteratively until convergence.

Further, we aim to maximize the NR BS coverage radius r of the NR BS such that a minimum SINR constraint is satisfied at the ES. To ensure robustness, the problem assumes a worst-case that all active users are positioned on the boundary of the BS's coverage area. The optimization problem is given by

$$\text{P5}: \underset{r,\delta_{m,n},P^{(N)}_{m,n},\forall m,n}{\text{maximize}} \quad r, \quad \text{s.t.}: \quad (C1)-(C6)$$

Section IV-A discusses their convexification, and the corresponding algorithms are then presented in Section IV-B.

IV. Proposed Methodology

A. Convexification of problems P2 and P3

To address the nonconvexity in P2, we first relax the binary variable $\delta_{m,n}$ to a continuous variable $0 \leq \delta_{m,n} \leq 1$, allowing fractional subcarrier assignments (to be projected/rounded after solving). In P2, the constraints $(C1)$, $(C2)$ are nonconvex constraints. The following lemma convexifies constraint $(C2)$.

Lemma 1: The SINR constraint $(C2)$ can be replaced with equivalent convex constraints $(C2a)$-$(C2e)$ given by

$$(C2a): \sum_{m,n} z_{m,n}\zeta_{m,n} \leq \mathcal{I}_{max}, \quad (C2b): z_{m,n} \leq P^{max}_{m,n}\delta_{m,n},$$
$$(C2c): z_{m,n} \leq P^{(N)}_{m,n}, \quad (C2d): z_{m,n} \geq P^{(N)}_{m,n} - P^{max}_{m,n}(1-\delta_{m,n}),$$
$$(C2e): z_{m,n} \geq 0, \tag{5}$$

where $z_{m,n} = \delta_{m,n}P^{(N)}_{m,n}$ and $P^{max}_{m,n}$ is the total power that can be allocated to the n^{th} subcarrier for the m^{th} user. The constraints in (5) are all convex in $z_{m,n}$, $P^{(N)}_{m,n}$, and $\delta_{m,n}$.

Proof: We express $\text{E}[|I_{s,k}|^2]$ as

$$\text{E}[|I_{s,k}|^2] = \tilde{G}^{(F)}_R |\mathcal{H}^{(BF)}(t)|^2 \sum_{m=1}^{M}\sum_{n=0}^{N} \delta_{m,n}P^{(N)}_{m,n}\zeta_{m,n}, \tag{6}$$

where $\zeta_{m,n} \triangleq \left| \int_0^{T^{(F)}} e^{\frac{j2\pi n\tau}{T^N_u}} p(\tau) \text{rect}\left(\frac{t-\ell T^{(\text{N})}_u + T^{(\text{N})}_g}{T^{(\text{N})}_{tot}}\right) d\tau \right|^2$ is a constant interference coupling factor from the n^{th} subcarrier of

Algorithm 1 Overall algorithm for distance minimization

1: Initialize $\delta_{m,n}^0$, $(P_{m,n}^{(N)})^0$, $(\mathrm{x}_F, \mathrm{y}_F)^0$, and set acceptable tolerance $\epsilon = 10^{-4}$, and iteration count $k = 0$.
2: **Repeat**
3: Fix $(\mathrm{x}_F, \mathrm{y}_F)^k$ and solve for $\delta_{m,n}^{k+1}, (P_{m,n}^{(N)})^{k+1}$ in P2a for RPO and P3a for SPO.
4: Fix $\delta_{m,n}^{k+1}, (P_{m,n}^{(N)})^{k+1}$ and solve for $(\mathrm{x}_F, \mathrm{y}_F)^{k+1}$ in P4.
5: Set $(\mathrm{x}_F, \mathrm{y}_F)^k, \delta_{m,n}^k, (P_{m,n}^{(N)})^k \leftarrow (\mathrm{x}_F, \mathrm{y}_F)^{k+1}, \delta_{m,n}^{k+1}, (P_{m,n}^{(N)})^{k+1}$.
6: Set $k = k + 1$, and calculate $\mathcal{F}$.
7: **Until** $\|\mathcal{F}^{k+1} - \mathcal{F}^k\| \leq \epsilon$.

the m^{th} user to the FSS receiver and can be computed offline. Thus, the SINR at ES becomes

$$\widetilde{\Gamma}^{(\mathrm{F})} = \frac{\mathcal{A}_1^2 |\mathcal{H}^{(\mathrm{F})}(t)|^2}{\sum_{m,n} \delta_{m,n} P_{m,n}^{(N)} \zeta_{m,n} + N_o^{(\mathrm{F})} \mathcal{B}^{(\mathrm{F})}}. \tag{7}$$

Since $(C2)$ is $\Gamma^{(F)} \geq \Gamma_{Th}$, we enforce

$$\widetilde{\Gamma}^{(\mathrm{F})} \geq \Gamma_{Th} \Leftrightarrow \sum_{m,n} \delta_{m,n} P_{m,n}^{(N)} \zeta_{m,n} \leq \mathcal{I}_{max}, \tag{8}$$

where $\mathcal{I}_{max} = \frac{\mathcal{A}_1^2 |\mathcal{H}^{(F)}|^2}{\Gamma_{Th}} - N_o^{(\mathrm{F})} \mathcal{B}^{(\mathrm{F})}$. (8) is still nonconvex as it has the product of variables, making it bilinear. We convexify it using McCormick envelopes by introducing a new variable $z_{m,n} = \delta_{m,n} P_{m,n}^{(N)}$ with the additional constraints. The new set of constraints, instead of $(C2)$, are obtained as (5). ■

Note that the objective function in P2 is concave in $P_{m,n}^{(N)}$. However, the problem arises due to the multiplication of $\delta_{m,n}$. By first order Taylor series approximation at the i^{th} iteration $(\delta_{m,n}^{(i)}, P_{m,n}^{(N)(i)})$, we get the linearized approximation as

$$\widehat{\mathcal{R}}_m^{(N)} = \sum_{n=1}^{N-1} \Big(\delta_{m,n}^{(i)} \Delta f_m \log_2 \Psi_{m,n} + \frac{\delta_{m,n}^{(i)} a_{m,n} (P_{m,n}^{(N)} - P_{m,n}^{(i)})}{\Psi_{m,n} \ln 2}$$
$$+ \Delta f_m \log_2 \Psi_{m,n} (\delta_{m,n} - \delta_{m,n}^{(i)}) \Big), \tag{9}$$

where $a_{m,n} = \frac{|\mathcal{H}^{(\mathrm{BN})}|^2}{N_0^{(N)}}$ and $\Psi_{m,n} \triangleq 1 + a_{m,n} \frac{P_{m,n}^{(i)}}{\Delta f_m}$. Then, $(C1)$ can be approximated to $\widehat{\mathcal{R}}_m^{(N)} \geq R_{Th}, \forall m$. As a consequence, the optimization problem in P2 can be approximated to

$$\text{P2a}: \underset{z_{m,n}, \delta_{m,n}, P_{m,n}^{(N)} \forall m,n}{\text{maximize}} \quad \sum_{m=1}^{M} \widehat{\mathcal{R}}_m^{(N)}$$
$$\text{s.t.}: (C1a): \widehat{\mathcal{R}}_m^{(N)} \geq R_{Th}, \forall m.$$
$$(C2a) - (C2e), (C3) - (C6).$$

Each iteration updates the expanding point $(\delta_{m,n}^{(i)}, P_{m,n}^{(N)(i)})$ and computes first-order Taylor approximation of the nonconvex constraint and objective, transforming the problem to the convex form solvable by the interior-point methods.

P3 shares P2's structure. By using Lemma 1 and variable substitution, we simplify $\Gamma^{(F)}$ to $\widetilde{\Gamma}^{(F)}$ and replace $(C2)$ with $(C2a) - (C2e)$. Similarly, $(C1)$ becomes $(C1a)$. Since $\widetilde{\Gamma}^{(F)}$ has the form $f(z) = \frac{c1}{a^T z + c2}$, it is concave in z as a decreasing convex function composed with an affine function. Thus, the objective is concave in $z_{m,n}$. We denote this approximated problem as P3a. Note that the approximation of $\Gamma^{(F)}$ by $\widetilde{\Gamma}^{(F)}$ is preserved in both problems P1 and P2, including in the objective function of P2.

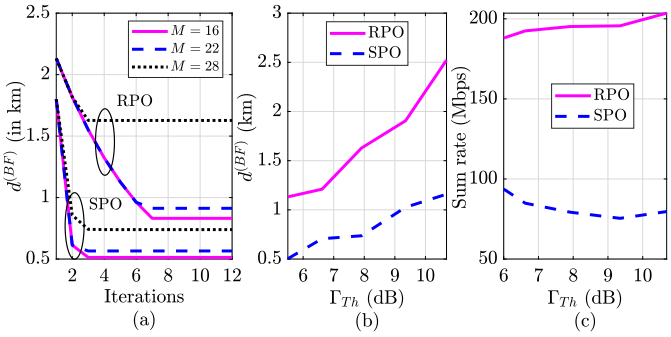

Fig. 3: Convergence and performance of the proposed approach.

B. Computational method for P4 and P5

In P4, the objective $d^{(\mathrm{BF})}$ is the Euclidean norm, i.e., a convex function of $\mathcal{X}^{\mathrm{U}}$. Its constraint $\Gamma^{(F)}$ is a decreasing function of $\mathrm{E}[|I_{s,k}|^2]$, depending upon the NR BS to ES distance. The interference $I_{s,k}$ involves the summation of NR waveforms passing through the NR-FSS channel $\mathcal{H}_k^{(BF)}(t)$, which is distance dependent, followed by matched filtering. Since, NR BS transmit an orthogonal subcarriers, noise and interference are uncorrelated, and the interference adds up due to multiple active subcarriers and spatial paths. We can approximate $\mathrm{E}[|I_{s,k}|^2] \approx \sum_{m=1}^{M} \sum_{n=1}^{N} \delta_{m,n} P_{m,n}^{(N)} (d^{(\mathrm{BF})})^{-\widetilde{\alpha}}$, where $\widetilde{\alpha}$ is the pathloss exponent, $P_{m,n}^{(N)} = \mathrm{E}[|x_m^{(N)}(t)|^2]$. Thus, $(C2)$ can be approximated to $\sum_{m=1}^{M} \sum_{n=1}^{N} \delta_{m,n} P_{m,n}^{(N)} (d^{(\mathrm{BF})})^{-\widetilde{\alpha}} \leq \mathcal{I}_{max}$. Since $\widetilde{\alpha} > 0$, $(d^{(\mathrm{BF})})^{-\widetilde{\alpha}}$ is convex. Since we have a convex constraint, the problem P4 is a convex optimization problem and is solved using interior point methods.

Algorithm 1 solves P1. Step 1 initializes $(P_{m,n}^{(N)})^0$, $\delta_{m,n}^0$, and $(\mathrm{x}_F, \mathrm{y}_F)^0$. Steps 2 to 7 perform alternating optimization, iteratively updating NR transmission parameters and ES location. The algorithm terminates when the change in the objective between iterations falls below the tolerance ϵ. The objective is $\mathcal{F} = \sum_{m=1}^{M} \widehat{\mathcal{R}}_m^{(N)}$ for RPO, or $\mathcal{F} = \widetilde{\Gamma}^{(\mathrm{F})}$ for SPO.

For P5, a bisection method is employed. At each step, P2a is solved to check feasibility under worst-case user placements. If the constraints are satisfied, r is feasible and the lower bound increases to search for larger valid radii. Otherwise, the upper bound decreases. The procedure terminates when the search interval is below tolerance ε.

Solving P2a or P3a using the interior point methods has complexity $C_a \triangleq \mathcal{O}((2MN)^{3.5} \log(1/\epsilon))$, where $2MN$ represents the number of variables to be optimized and ϵ represents the solution accuracy. Similarly, P4 has complexity $C_b \triangleq \mathcal{O}(3^{3.5} \log(1/\epsilon))$. Let I_{iter} denote the outer iterations for alternating scheme convergence; the overall distance optimization complexity is $\mathcal{O}(I_{iter} \max\{C_a, C_b\})$. P5 complexity depends on iterations to feasibility. Let $\bar{r}_{\max}$ denote these iterations. The total cost of P5 is approximately $\mathcal{O}(\bar{r}_{\max} (2MN)^{3.5} \log(1/\epsilon))$.

V. Numerical Results

The key FSS and NR parameters are taken from [14]. Unless stated otherwise, the NR parameters are set to $N = 601$ and $P_{\max} = 40$ W. Specifically, $\tilde{\alpha} = 2.3$ corresponds to RMa

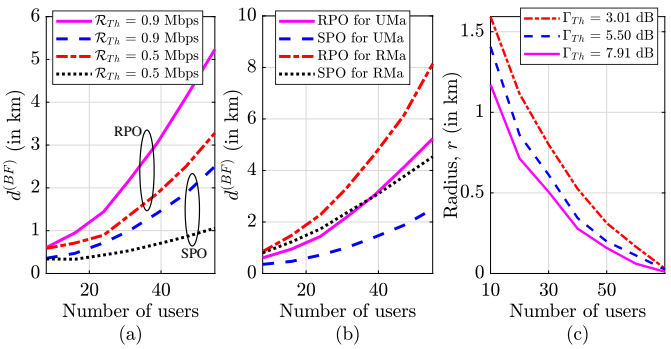

Fig. 4: Impact of the number of active users on the NR BS coverage.

scenario, and $\tilde{\alpha} = 3$ corresponds to UMa scenario. These values are consistent with the empirical parameters widely adopted in C-band propagation studies [13].

Fig. 3(a) shows the convergence of NR BS-ES distance $d^{(\mathrm{BF})}$ over the alternating optimization for $M = \{16, 22, 28\}$, with $\mathcal{R}_{\mathrm{Th}} = 0.9$ MHz, $\Gamma_{\mathrm{Th}} = 7.91$ dB. Both RPO and SPO converge within a few iterations. Fig. 3(b) compares RPO and SPO for different SINR threshold Γ_{Th} ($\mathcal{R}_{\mathrm{Th}} = 0.75$ MHz, $\lambda = 10^{-5}$ users/m^2). As Γ_{Th} increases, $d^{(BF)}$ grows for both strategies. RPO shows a steeper distance increase by prioritizing NR performance at the cost of higher ES interference. SPO achieves smaller BS-ES distance by allocating fewer resources, enabling more compact deployments. Fig. 3(c) shows that SPO yields a lower sum rate, decreasing slightly with increasing Γ_{Th}, owing to stricter interference constraints.

Fig. 4(a) shows the impact of users (M) on protection distance (for different $\mathcal{R}_{\mathrm{Th}} = \{0.5, 0.9\}$ MHz, $\Gamma_{\mathrm{Th}} = 7.91$ dB) for both strategies. For RPO, the optimal BS-ES distance increases significantly with M, reaching up to approximately 5 km, as more users require greater resources, increasing ES interference. RPO activates all $N = 601$ subcarriers regardless of M, whereas SPO uses fewer subcarriers (366 for $M = 22$), only increasing modestly with user demand to limit ES interference. Fig. 4(b) shows the comparison of d^{BF} for two different scenarios (UMa and RMa). It can be observed that for RMa, protection distance increases compared to UMa due to lower path loss exponent and reduced blockage density in rural environments. In contrast, the higher attenuation and dense scattering in UMa environments confine the interference footprint, resulting in a smaller protection distance.

Fig. 4(b) illustrates the effect of M on the worst-case coverage radius r for different Γ_{Th} ($\mathcal{R}_{\mathrm{Th}} = 0.75$ Mbps, $P_{\max} = 40$ W, and $N = 601$ subcarriers; the ES at coordinates $(-900, 10, 5)$ m). As M increases, the coverage radius r decreases across all SINR thresholds due to more stringent power sharing and higher aggregate interference toward the ES. Higher SINR constraint (e.g., $\Gamma_{\mathrm{Th}} = 7.91$ dB) imposes tighter interference control, forcing users closer to the BS. For large M and high Γ_{Th}, feasible r can shrink to as little as 16 m, creating impractical deployments.

Remark: The proposed framework is valuable for mobile network operators and is applicable in both pre-deployment phase (guiding optimal BS placement) and post-deployment phase (enabling real-time NR transmission parameter optimization). From an operator's perspective, results provide practical guidelines for balancing NR performance and FSS protection through power control and subcarrier activation.

VI. Conclusion

We proposed an interference-aware coexistence strategy exploiting NR flexibility to enable NR-FSS coexistence in the C-band. A nonconvex optimization problem was formulated to minimize NR BS-ES distance by jointly optimizing NR transmission parameters and NR BS location, solved via two-stage decomposition. First, SPO employs conservative spectrum usage to mitigate ES interference, achieving smaller BS-ES distance than RPO at the cost of lower NR performance. Second, we analyzed worst-case NR coverage radius satisfying ES SINR constraints, demonstrating practical deployment feasibility. The proposed SPO strategy achieves interference suppression but exhibits some limitation in terms of low NR resource utilization, which highlights the need for a more flexible coexistence mechanism. Joint optimization of NR transmission parameters and adaptive guard band coordination would be of interest as a future work to achieve more efficient coexistence between NR and FSS systems.

References

[1] Int. Telecommun. Union, Radiocommunication (ITU-R), "Sharing studies between IMT-Advanced systems and geostationary satellite networks in the fixed-satellite service in the 3 400-4 200 and 4 500-4 800 MHz frequency bands," ITU-R, Tech. Rep. M.2109, 2007.

[2] H. Tan, Y. Liu, Z. Feng, and Q. Zhang, "Coexistence analysis between 5G system and fixed-satellite service in 3400–3600 MHz," *China Commun.*, vol. 15, no. 11, pp. 25–32, Nov. 2018.

[3] S. Kaya, A. Knopp, T. Hälsig, and K.-U. Storek, "Channel estimation improved 5G interference canceling at satellite ground stations: Initial results," in *Proc. IEEE ICC*, May 2023, pp. 6671–6676.

[4] G. Castellanos, G. Teuta, H. P. Penagos, and W. Joseph, "Coexistence for LTE-advanced and FSS services in the 3.5 GHz band in colombia," in *Proc. Adv. Satellite Multimedia Sys. Conf. and Sig. Process. Space Commun. Wksp. (ASMS/SPSC)*, Oct. 2020, pp. 1–7.

[5] S. Liu, Y. Wei, and S.-H. Hwang, "Guard band protection for coexistence of 5g base stations and satellite earth stations," *ICT Express*, vol. 9, no. 6, pp. 1103–1109, Dec. 2023.

[6] E. Lagunas, C. G. Tsinos, S. K. Sharma, and S. Chatzinotas, "5G cellular and fixed satellite service spectrum coexistence in C-Band," *IEEE Access*, vol. 8, pp. 72 078–72 094, 2020.

[7] C. Muhammad and K. Anwar, "Interference mitigation using adaptive beamforming with RLS algorithm for coexistence between 5G and fixed satellite services in C-band," in *J. Physics: Conf. Series*, vol. 1577, no. 1, Jul. 2020, p. 012029.

[8] S. Kim, E. Visotsky, P. Moorut, K. Bechta, A. Ghosh, and C. Dietrich, "Coexistence of 5G with the incumbents in the 28 and 70 GHz bands," *IEEE J. Sel. Areas Commun.*, vol. 35, no. 6, pp. 1254–1268, Apr. 2017.

[9] X. Liu, K.-Y. Lam, F. Li, J. Zhao, L. Wang, and T. S. Durrani, "Spectrum sharing for 6g integrated satellite-terrestrial communication networks based on noma and cr," *IEEE Network*, vol. 35, pp. 28–34, Aug. 2021.

[10] Z. Li, S. Han, L. Xiao, and M. Peng, "Cooperative non-orthogonal broadcast and unicast transmission for integrated satellite-terrestrial network," *IEEE Trans. Broadcast.*, vol. 70, pp. 1052–1064, Dec. 2024.

[11] Y. Wu, F. Zhou, W. Wu, Q. Wu, D. W. K. Ng, and T. Q. Quek, "Robust resource allocation for RSMA spectrum sharing networks," *IEEE Trans. Wireless Commun.*, vol. 23, no. 11, pp. 16 375 – 16 389, Nov. 2024.

[12] A. Girdher, S. De, J.-B. Seo, and R. K. Mallik, "In-band coexistence of new radio with fixed satellite services in C-band," in *Proc. IEEE ICC Wksp.*, Montreal, Canada, Jun. 2025, pp. 1–6.

[13] "5G: Study on channel model for frequencies from 0.5 to 100 GHz," 3GPP TR 38.901 ver. 16.1.0 Rel. 16, Nov. 2020.

[14] "5G; NR; base station (BS) radio transmission and reception," 3GPP TS 38.104 ver. 16.4.0 Rel. 16, Jul. 2020.